



Synthesis and Characterization of Chitosan/ZrO₂ Nanocomposite and Its Application in the Removal of Rose Bengal Dye

Ahmed A. Thabet^a, Ahmed S. Elfeky^a, Wael S. Mohamed^b, Ahmed S. Elzaref^a, Zeinhom M. El-Bahy^a



CrossMark

^aChemistry Department, Faculty of Science, Al-Azhar University, Nasr City, P.B. 11884, Cairo, Egypt.

^bDepartment of Polymers and Pigments, National Research Centre, 33 Bohouth st., Dokki, 12622, Giza, Egypt

Abstract

The removal of Rose Bengal dye (RB) from aqueous solution was tested by the adsorption process at initial dye concentration in the range of 3–50 ppm. For this purpose, a novel and sustainable Chitosan/Zirconium oxide nanocomposite (CS/ZrO₂ NCs) was prepared by incorporating Zirconium oxide nanoparticles (ZrO₂ NPs) into Chitosan nanoparticles (CS NPs). The prepared CS/ZrO₂ NCs samples were characterized by many spectral techniques such as XRD, FTIR, SEM, EDX and TEM. The adsorption conditions such as dye concentration, contact time and CS/ZrO₂ mass ratios were optimized. The experimental data shows that CS/ZrO₂ containing 30% of ZrO₂ NPs (CS/ZrO₂ (30%)) has the highest adsorption capacity for eliminating RB dye among all the prepared samples. The maximum dye removal efficiency increased from 46% for Chitosan to 78% for the sample containing 30% of ZrO₂ in CS/ZrO₂ NCs. Isotherm models such as Langmuir and Freundlich were analysed. Kinetic studies indicated that Freundlich isotherm and pseudo-second order models are the best fitting for our experimental results.

Keywords: Chitosan, ZrO₂, adsorption, Isotherm, Kinetics

1. Introduction

The purity of water became an important issue due to industrialization activities. Fresh water that presents on the earth's surface is subjected to many uses and demands. It is used for drinking, domestic and municipal uses, agricultural, irrigation, industries, navigation, and recreation. Water gets easily polluted because it has the ability to dissolve more substance than any other solvent. The used water becomes contaminated and is called wastewater [1]. Water pollution became one of the major environmental challenging problems faced by the world and it can be defined as alteration in physical, chemical, or biological characteristics of water through natural or human activities and making it unsuitable for its designated use. Major parts of the contaminants are coming from different industry containing heavy metals, hazardous dyes, radioactive pollutants, toxic chemicals, fluoride etc. Some industrial activities such as textile, colouring, cosmetic, paint, food, paper, printing, and pharmaceuticals are considered as a big demand from the environmental point of

view because many hazardous synthetic dyes are generally heavily produced [2].

The biodegradation of organic dyes is difficult due to its aromatic molecular structure. Organic dyestuffs in wastewater of many industries are extensively discharged to the environment affording serious soil and water pollution due to biological degradation, high chemical oxygen demand (COD) of water and inflicted toxicity on humans [3]. On the basis of a survey, it has been reported that textile industry, pharmaceutical factory, leather industry, plastic industry disposed 50000 tons of dyes per year to the water bodies. The industrial dye compounds prevent the sunlight and afford hazard damage to aquatic and human life. So many techniques are being used to improve the traditional water treatment processes including physical processes or chemical treatments [4-6]. Adsorption is the most effective and broadly utilized technique. The most important advantages of adsorption are its relatively low cost and its ease implementation of the operation process. The effectiveness of the adsorption process depends on the performance of the adsorbent material [7].

*Corresponding author e-mail: wsabry1976@yahoo.com

Receive Date: 07 February 2022, Revise Date: 13 March 2022, Accept Date: 22 March 2022

DOI: 10.21608/EJCHEM.2022.120576.5408

©2022 National Information and Documentation Center (NIDOC)

Recently, many adsorbents such as activated carbon [8-10], barium phosphate [11], carbon nanotube [12], alginate bead [13], smectites [14], graphene [15], zeolite [16] and polysaccharides [17] have been widely used for dye removal but most of them have one or more disadvantages such as low adsorption capacity, high cost, unsatisfactory separation and the need for large amounts of adsorbent.

Due to some disadvantages in all dye degradation methodologies, attention toward chitosan-based adsorbents has increased for the adsorption of dyes. Chitosan is a biodegradable [18], nontoxic [19], natural polysaccharide [20-23] and one of the readily available polymers with relatively high abundance and sustainable materials with divergent functional groups that are employed in broad range of applications [24]. It is derived by deacetylation of chitin which is one of the most profuse natural poly saccharides [25]. It has antibacterial activity and binding tendency with pollutants which facilitate the efficient adsorption process in water treatment. Additionally, it is biocompatible, biodegradable, less toxic, and convenient in chemical modifications, which exhibit high adsorption abilities in neutral solution [26]. Many research works reported that the interaction of primary amine group in chitosan with various groups through 3-D network formation can improve the mechanical stretch and adsorption ability of chitosan-based polymer nano composite. Although chitosan has many advantages, it is still needed to enhance its catalytic activity and adsorption efficiency [14, 27]. Combining chitosan, and other reactive materials with a selective affinity toward anions sorption would constitute a viable approach to develop multi-functional composites to simultaneously remove both cations and anions from water.

Zirconium oxide is a physically rigid material with chemical inertness. It's a harmless element with good stability, cheap and eco-friendly material. It has high resistance against attacks by acids, alkalis, oxidants and reductants [28, 29], so Zirconium oxide-based materials are used in many applications including automobile engine parts, wire-drawing dies, and cutting tools. Additionally it's used in dye removal by adsorption and photocatalysis methods [29, 30]. Metal oxide nanoparticles (MONPs) have unique properties differ from their properties in large scale [31]. However, they can easily coagulate when applied directly. This problem can be solved by introducing a suitable carrier or stabilizer [32].

In the present work, to develop nanocomposite with high efficiency towards dye removal, Chitosan nanoparticles and Chitosan/ZrO₂ nanocomposite (CS/ZrO₂ NCs) were prepared with different ratio of dopant metal oxide. The synthesized nanocomposite was characterized by several spectral techniques FTIR, SEM-EDX, XRD and TEM analysis. Removal

of hazardous Rose Bengal dye were optimized according to percentage of metal oxide doped on pristine material, the initial concentration of dye and contact time. Adsorption models were applied, and thermodynamic parameters were calculated.

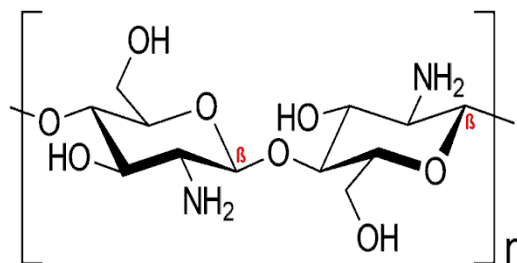
2. Materials and methods

2.1. Materials

Chitosan (degree of deacetylation: >75 %, average molecular weight: 200 kDa and chemical structure shown in Scheme 1), Sodium Tripolyphosphate (STPP), sodium hydroxide, Acetic acid, Rose Bengal dye (C₂₀H₂Cl₄I₄Na₂O₅) and Zirconium (IV) oxide (ZrO₂ nano powder with size <100 nm) were purchased from Sigma-Aldrich.

2.2. Preparation of Chitosan nanoparticles

Chitosan (CS) nanoparticles were prepared by dissolving chitosan at the concentration of 0.5% (W/V) in acetic acid 1% (V/V) and then the pH was adjusted at 4.6-4.8 by adding 1N NaOH. Chitosan NPs were shaped spontaneously after addition of 3 ml of 0.25 % (W/V) of aqueous sodium tripolyphosphate solution under continuous magnetic stirring. The nanocomposites were purified by centrifugation at 9000 rpm for 30 min. Supernatants were discarded, and the chitosan nanoparticles were extensively rinsed with de-ionized distilled water to remove any sodium hydroxide and thereafter freeze dried before further use and analysis [33].



Scheme (1): Structure of Chitosan

2.3. Preparation of Chitosan-ZrO₂ Nanocomposite

Different amounts of ZrO₂ were sonicated in CS nanoparticles solution (2% w/v in acetic acid 1% v/v) for 20 min then the suspension was stirred for 8 h at room temperature (25°C), washed with ultrapure water by ultracentrifugation to remove unbound CS, and dried at room temperature to obtain CS-ZrO₂ nanocomposites with different ZrO₂ percentage [34]. The final composite nanoparticles (CNPs) were referred as CS/ZrO₂ (1%), CS/ZrO₂ (10%), CS/ZrO₂ (20%), CS/ZrO₂ (30%), CS/ZrO₂ (40%) and CS/ZrO₂ (60%), where the subscript number between brackets refers to the ZrO₂ percentage.

2.4. Characterization of Chitosan/ZrO₂ nanocomposite

Characterization of the catalysts was performed using several methods. X-ray diffraction (XRD) was carried out using (X PERT PRO – PAN Analytical) diffractometer with Cu radiation and a 2θ range of 4–80°. Fourier transfer infrared (FTIR) spectrum was recorded by BRUKER Spectrum using attenuated total reflectance mode, in the wave number range of 400–4,000 cm⁻¹. Scanning electron microscopy (SEM-EDX) analysis was carried out using Quanta FEG 250/EDAX with field emission gun, FEI company – Netherlands) to investigate the surface morphology of the composites. Transmission electron microscopy (TEM) was carried out using TEM (JEOL JEM 2100, Tokyo, Japan), where the suspension of the material was sonicated for 10 minutes (crest Ultrasonics Crop., New Jersey, USA). Few drops were loaded on carbon coated copper grid, left to dry and then the grid-loaded sample was examined.

2.5. Adsorption experiments

RB dye (Scheme 2) removal efficiency by using Chitosan, ZrO₂ and CS/ZrO₂ nanocomposite was applied by comparing the adsorption of Rose Bengal dye with the time. To perform the experiments, 100 ml of 50 mg L⁻¹ dye solutions were added into 0.1 g of catalyst. The solution was mixed in dark for 60 min to achieve adsorption-desorption equilibrium. Samples (2 ml) were regularly collected at different time intervals and analyzed by UV-visible spectrophotometer.

In order to investigate the effect of Chitosan/ZrO₂ mass ratios on the sorption of RB dye, various mass ratios of (Chitosan/ZrO₂) were used (over a range of 1%, 10%, 20%, 30%, 40% and 60% ZrO₂). The experiments were conducted for 60 min in 100 ml solution containing 50 mg L⁻¹ RB dye using 0.1 g composites. Also to investigate the effect of initial dye concentration, adsorption isotherm experiments were carried out for 30 min by changing initial concentrations of RB dye over a range of 50, 30, 15, 7 and 3 mg L⁻¹, at a fixed adsorbent dose of 0.1 g.

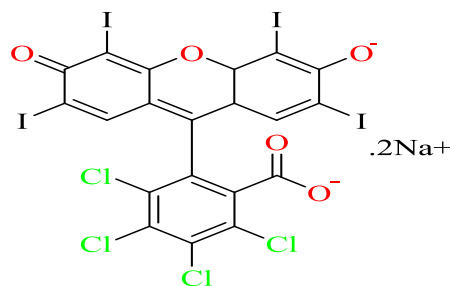
To determine the amount of eliminated dye from aqueous solution the suspension was filtered, and the supernatant was analyzed using Lambda UV/vis spectrophotometer (Perkin Elmer). The adsorption capacity and dye removal percent were calculated using the following expressions (Eqs. 1 and 2):

$$qt = \left(\frac{C_0 - Ct}{M} \right) V \text{ ----- (1)}$$

$$\text{Dye removal \%} = \left(\frac{C_0 - C_e}{C_0} \right) * 100 \text{ ---- (2)}$$

Where C₀ is the initial concentration, C_e is the equilibrium concentration and C_t amount of adsorbed

dye. V is the volume of RB dye solution and M is the adsorbent weight. The adsorption isotherms and kinetic models were applied to calculate the different parameters and select the best model for the adsorption process.



Scheme (2) Structure of Rose Bengal dye

3. Results and Discussion

3.1. Characterization of Chitosan/ZrO₂ nanocomposite

3.1.1 X-ray diffraction

The XRD spectra of Chitosan, ZrO₂ and CS/ZrO₂ (30%) NCs were shown in Fig. (1). Chitosan, Fig. (1a), showed a broad peak at 2θ = 20° with small peak at 2θ = 47° which are corresponding to a crystalline structure of Chitosan [19]. Whereas, XRD spectrum of ZrO₂ is presented in Fig. (1b) and showed five bands at 2θ = 16.39°, 19.22°, 24.82° and 30.68°. These signals are assigned to ZrO₂ structure [35, 36]. The XRD spectrum of CS/ZrO₂(30%), Fig (1c), showed peaks at 2θ = 12.57°, 16.34°, 18.79°, 20.42°, 25.06°, 29.87°, 31.64°, 38.53°, 39.26°, and 62.41° after loading with ZrO₂ with extraordinary broadness in the peak. The peak at 2θ = 20.42° was overlapped by that of raw Chitosan. The results may indicate the incorporation of ZrO₂ into Chitosan.

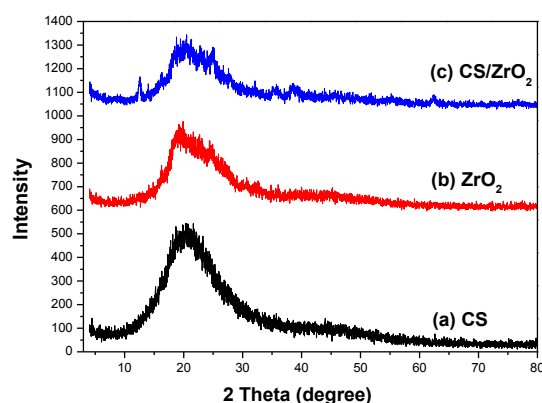


Figure (1): XRD spectra of Chitosan (a), ZrO₂ (b) and CS/ZrO₂ (30%) NCs (c)

3.1.2. Fourier transfer infrared (FTIR)

The obtained FTIR spectral results for Chitosan, ZrO₂ and CS/ZrO₂ (30%) NCs are presented in Fig. (2), and

has been obtained in the range of 4000–400 cm^{-1} . Fig. (2) Shows different bands around 3330, 2920, 2870, 2360, 1640, 1380, 1110, 675 and 478 cm^{-1} . The band around 3330 cm^{-1} is typically associated to the hydroxyl group [27], whereas, that found near 1640 cm^{-1} is related to the bending vibration of adsorbed water hydroxyl [27]. Bands near 2920, 2870, 1380 and 1110 cm^{-1} are assigned to Chitosan [19], meanwhile, that around 675 and 478 cm^{-1} are related to ZrO_2 and band at 2360 cm^{-1} is related to stretching vibration of hydroxyl zirconium (Zr–OH) bond [36]. In Fig. (2), there is a slight shifting in some peaks and transmittance percentages (%T) of waves duo to incorporation of ZrO_2 into Chitosan.

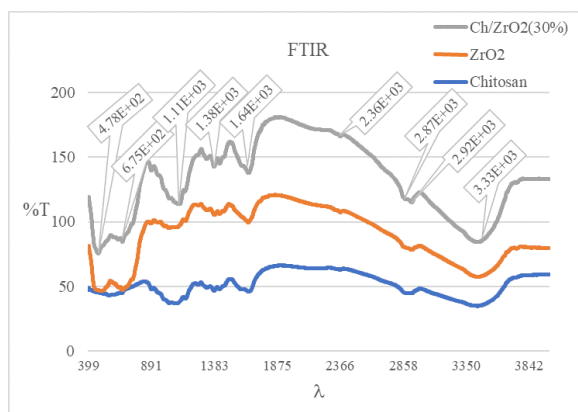


Figure (2): FTIR spectra of Chitosan (a), ZrO_2 (b) and CS/ZrO_2 (30%) NCs (c)

3.1.3. SEM-EDX and TEM analysis

The morphologies and microstructures of prepared samples were studied via high resolution scanning electron microscope (SEM) and Transmission electron microscopy (TEM) analyses. SEM images of Chitosan, ZrO_2 and CS/ZrO_2 (30%) NCs composites were represented in Fig. (3a-c). the SEM images data (at magnification 5 μm) shows that pure Chitosan in Fig. (3a) has an average size of 80–110 nm. Fig. (3b) shows that pure ZrO_2 presented an irregular particle with an average size of 56–89 nm. Fig. (3c) shows Chitosan/ ZrO_2 (30%) NCs where composite materials, chitosan and ZrO_2 were tightly coupled together with an average size of 31–44 nm. The TEM technique was used to further explore the microstructures of the prepared samples. The TEM images of pure Chitosan is shown in Fig. (3d) and Chitosan/ ZrO_2 (30%) NCs is shown in Fig. (3e). the data shows the prepared samples form a small aggregation with an average size in the range of 21–109 nm for pure Chitosan and 55–92 nm for Chitosan/ ZrO_2 (30%) NCs. These size range indicates that the prepared samples are obtained which reflects the high surface areas of the nano particles that increases the efficiency of their

removal capacities. The Energy Dispersive X-ray spectroscopy (EDX) analysis of ZrO_2 were represented in Fig. (3f) confirmed the presence of Zr and O.

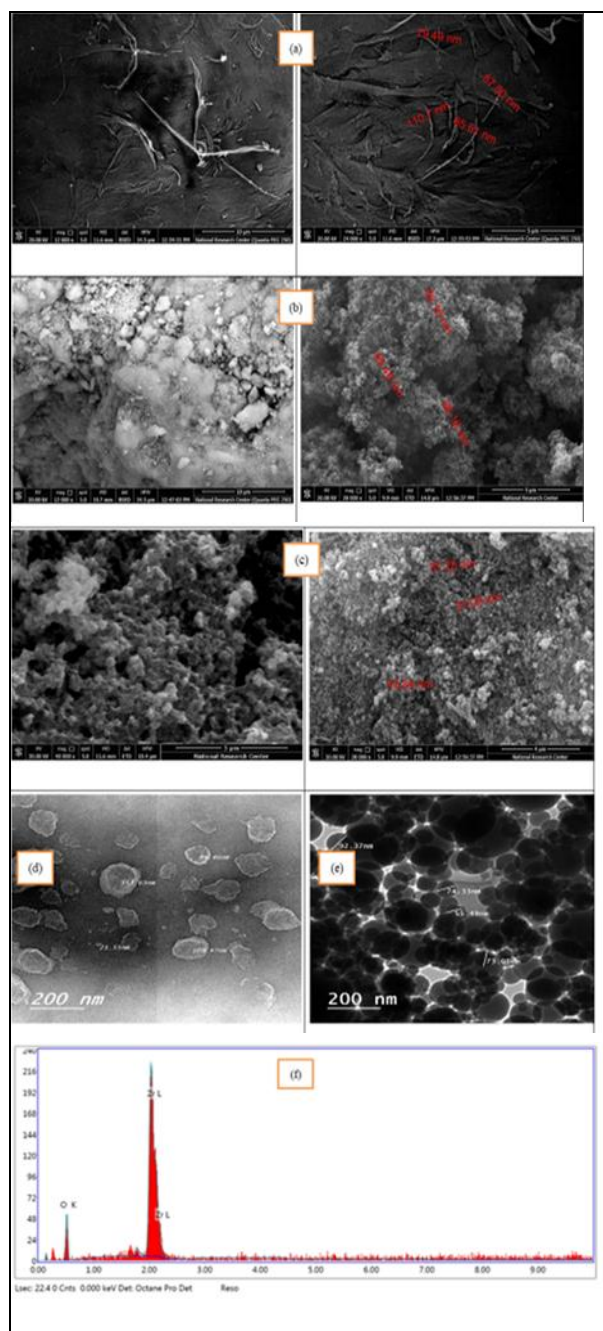


Figure (3): SEM spectra of Chitosan (a), ZrO_2 (b) and CS/ZrO_2 (30%) NCs (c), TEM of Chitosan (d) and CS/ZrO_2 (30%) NCs (e), EDX of ZrO_2 (f).

3.2 Adsorption of Rose Bengal dye over the prepared nanocomposites

3.2.1 Effect of Chitosan/ ZrO_2 mass ratios

The removal of Rose Bengal dye by CS/ZrO_2 NCs at different mass ratios is shown in Fig. (4). It was

found that, the increase in the mass ratio of ZrO₂ lead to a gradual increase of dye removal until reaching CS/ZrO₂(30%) which shows the highest adsorption efficiency. The dye removal efficiencies of Chitosan, ZrO₂, CS/ZrO₂ (1%), CS/ZrO₂ (10%), CS/ZrO₂ (20%), CS/ZrO₂ (30%), CS/ZrO₂ (40%) and CS/ZrO₂ (60%) were found to be 46%, 22%, 60%, 66%, 73%, 78%, 56% and 51%, respectively. The data show that the removal % approaches 46% over nano-chitosan and increased to 78% over CS/ZrO₂ nanocomposites with increasing mass ratio of ZrO₂ to 30% which is considered as the optimum ZrO₂ ratio. The increase in the removal efficiency of the dye up to 30% loads of ZrO₂, may imply the enlargement of Chitosan specific surface areas by providing of more active centres of ZrO₂ nanoparticles to the sum of internal surface areas of the original porous structure.

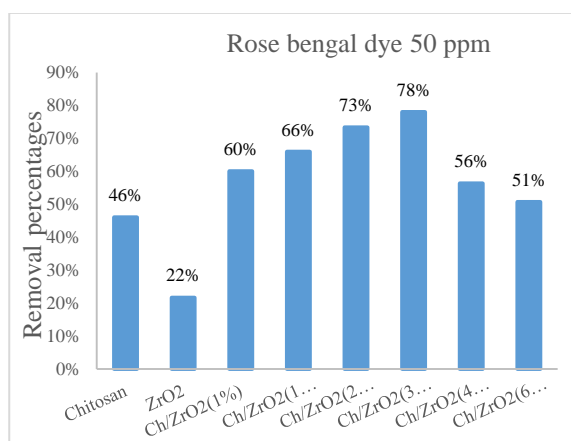


Figure (4): Effects of CS/ZrO₂ mass ratios on removal of RB dye

The increase in the mass ratio of ZrO₂ more than 30% leads to a decrease of dye removal efficiency, which may be due to the possible tendency of aggregation of ZrO₂ nanoparticles on some Chitosan surface sites. Consequently, ZrO₂ NPs may mask some of the adsorption active sites and hinder the removal of dye. Because CS/ZrO₂ (30%) sample shows the highest adsorption efficiency for RB dye, it was used for all the studies below.

3.2.2 Effect of initial dye concentration:

Removal of Rose Bengal dye by CS/ZrO₂ (30%) NCs composites at different initial dye concentration is shown in Fig. (5). Initial RB dye concentrations were changed between 3 to 50 mg L⁻¹. The dye removal of 3 mg L⁻¹ solution was found as 91%, while it was 85%, 80%, 73% and 72% for 7, 15, 30 and 50 mg L⁻¹, respectively.

The difference between the removal percentages depends on the occupation of active sites by the adsorbate molecules. Certain numbers of active sites on catalyst were occupied by RB dye molecules and could be shielded by dye molecule at higher

concentration, which causes a decrease on dye removal.

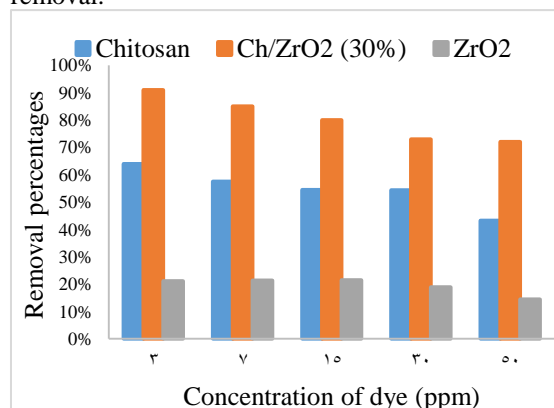


Figure (5): Effect of initial dye concentration removal using Chitosan, CS/ZrO₂ (30%) and ZrO₂

3.2.3 Effect of contact time:

Removal of Rose Bengal dye (50 ppm) by (0.1 g) CS/ZrO₂ (30%) NCs composites at 60 min is shown in Fig. (6). the removal of RB dye by CS/ZrO₂ (30%) NCs catalyst was 47% in first 5 min. and reached 78% in 60 min. The removal efficiency becomes constant and negligible after 60 min. The high efficiency of the CS/ZrO₂ (30%) in removing dye at early stage, may be explained by the combined effect of the enrichment of CS/ZrO₂ (30%) NCs adsorption sites, along with the initial high concentration of the adsorbate. At later stages of the test, the reduction of uptake capacity may be attributed to the blocking effect of the pores and channels by dye molecules accumulation which results in slower rate of dye diffusion into the majority of the adsorbents.

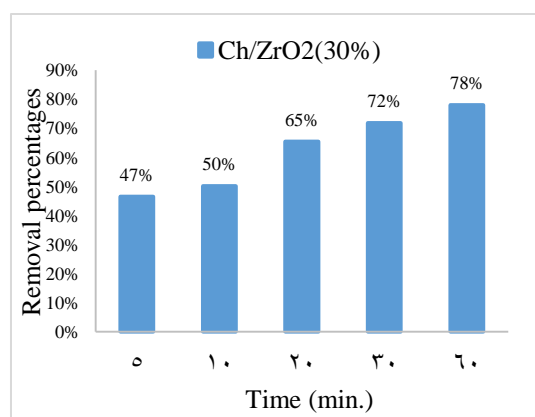


Figure (6): removal percentages of RB dye at different times

3.2.4 Adsorption isotherms

Langmuir [37] and Freundlich [38] model's equations in Table (1) are commonly used to describe the adsorption isotherms for application in the wastewater treatment design. Experimental and theoretical adsorption isotherms for the chitosan, ZrO₂ and CS/ZrO₂ NCs.

(Table 1) Kinetic equations.

Model	Equation	Eq. no.
Freundlich	$\ln q_e = \ln K_f + \frac{1}{n} \ln C_e$	1
Langmuir	$\frac{C_e}{q_e} = \frac{1}{KLQ_{max}} + \frac{C_e}{Q_{max}}$	2
	$R_L = \frac{1}{1 + KLC_0}$	3
Pseudo-first-order	$\ln(q_e - q_t) = \ln q_{e,1} - K_1 t$	4
Pseudo-second-order	$\frac{t}{qt} = \frac{1}{K_2 qe_2} + \frac{1}{qe} t$ $h = K_2 qe_2$	5
Intraparticle diffusion	$q_t = k_{ipd} t^{0.5} + C$	6
Liquid film diffusion	$\ln(1 - F) = -k_{fd} t + C$ $f = q_t / q_e$	7

(Table 2) The Nomenclature of the equations constant.

q_e	Amount of solute sorbate at equilibrium (mmol g ⁻¹)
q_t	Adsorbed amount at time (t)
C_e	Equilibrium concentration of adsorbate (mmol L ⁻¹)
C_0	Initial metal ions concentration (mmol L ⁻¹)
K_f	Multilayer adsorption capacity (mmol g ⁻¹)
n	Freundlich isotherm constants
Q_{max}	Theoretical maximum adsorption capacity (mmol g ⁻¹)
K_L	Energy of adsorption (L mmol ⁻¹)
R_L	Separation factor
$q_{e,1}$ $q_{e,2}$	Amount of solute sorbate on the surface of the adsorbent at equilibrium and at any time t (mmol/g).
K_1	k_1 (gm mmol ⁻¹ min ⁻¹) is pseudo-first order rate constant at equilibrium
K_2	K_2 (min ⁻¹) is pseudo-first order rate constant at equilibrium
t	Time (min.)
h	Initial adsorption rate (mmol g ⁻¹ min ⁻¹)
K_{ipd}	Intraparticle diffusion rate coefficient (mmol g ⁻¹ min ^{-0.5})
$t^{0.5}$	Half life time
C	Thickness of the boundary layer (mmol g ⁻¹)
F	kfd are fractional attainment of equilibrium and film diffusion rate constant
K_{fd}	Film diffusion rate coefficient

Freundlich isotherm

For a favourable adsorption process n should be more than 1 [39]. The Freundlich constant, K_f , (adsorption capacity) value was increased with CS/ZrO₂ NCs. The n values at equilibrium are greater than 1, reflecting a favourable adsorption in three samples. The results indicated that the chitosan, ZrO₂ and CS/ZrO₂ NCs have strong adsorption capacity for RB dye in solution.

Langmuir isotherm

The theoretical maximum adsorption capacity (q_{max}) values were 35.97, 17.15 and 46.73 mg/g for chitosan, ZrO₂ and CS/ZrO₂ NCs, respectively. The value of separation factor R_L indicates the type of the adsorption isotherm to be either unfavourable ($R_L > 1$), linear ($R_L = 1$), favourable ($0 < R_L < 1$) or irreversible ($R_L = 0$). The R_L values reported in Table (3), show that the behaviour of RB dye adsorption chitosan, ZrO₂ and CS/ZrO₂ NCs were favourable ($0 < R_L < 1$). The regression coefficients were very close to unity namely, $R^2 = 0.9852, 0.9816$ and 0.9985 for chitosan, ZrO₂ and CS/ZrO₂ NCs, respectively, Table (3). These data show the well-fitting of adsorption data for RB dye to Freundlich model, as compared to Langmuir isotherm.

Adsorbent	Chitosan	ZrO ₂	CS/ZrO ₂	
Langmuir parameters	Q_0 (mg/g)	35.97	17.15	46.73
	K_1 (L/mg)	0.0481	0.0179	0.1467
	R_L	0.29	0.53	0.12
	R^2	0.9021	0.8615	0.8917
Freundlich parameters	n	1.3	1.16	1.55
	K_f (mg/g)	1.853	0.335	6.056
	R^2	0.9852	0.9816	0.9985

(Table 3) Adsorption isotherm parameters RB on chitosan, ZrO₂ and CS/ZrO₂ NCs in aqueous solution.**3.2.5 Adsorption kinetic models**

Kinetic models can be helpful in understanding the mechanism of sorption and evaluating the

performance of the adsorbent. In the present study, the sorption kinetic data were analyzed by pseudo-first-order [40], pseudo-second-order [41], intraparticle diffusion [42] and liquid film diffusion [43]. The kinetic model's data are presented in Table (4).

The pseudo-first order rate equation was proposed by Lagergren [16] and is widely used for the adsorption of liquid/solid system. The pseudo-first order plots for RB dye on surface of chitosan, ZrO₂ and CS/ZrO₂ NCs, are shown in Fig. (7-a). The values of the adsorption rate constant (k_1) for RB dye obtained from the straight-line plot were 0.116, 0.70 and 0.06 min⁻¹ for chitosan, ZrO₂ and CS/ZrO₂ NCs, respectively at initial RB dye concentration of 3 ppm. The values of correlation coefficients were 0.79, 1.00 and 0.78 for chitosan, ZrO₂ and CS/ZrO₂ NCs, respectively. But the values of the amount of solute sorbate at equilibrium (q_e) calculated from this straight line differed appreciably from the values of q_e obtained experimentally. Therefore, pseudo-first order kinetic model described RB dye adsorption, whereas RB dye adsorption did not follow pseudo first order kinetics.

Pseudo-second order model suggests that both number of adsorption sites on the material surface and concentration of adsorbate ions in the liquid phase determine the rate. Pseudo-second order plots for chitosan, ZrO₂ and CS/ZrO₂ NCs are shown in Fig. (7-b). The values of k_2 for chitosan, ZrO₂ and CS/ZrO₂ NCs adsorption were found to be 0.509, 16.58 and 0.13 g/mg min, respectively at 3 ppm. The regression coefficient values Table (3) for, chitosan ZrO₂ and CS/ZrO₂ NCs were 1.00, 1.00 and 0.91 at 3 ppm, which indicated the better suitability of pseudo-second order kinetics in the adsorption process, as compared to pseudo-first order model.

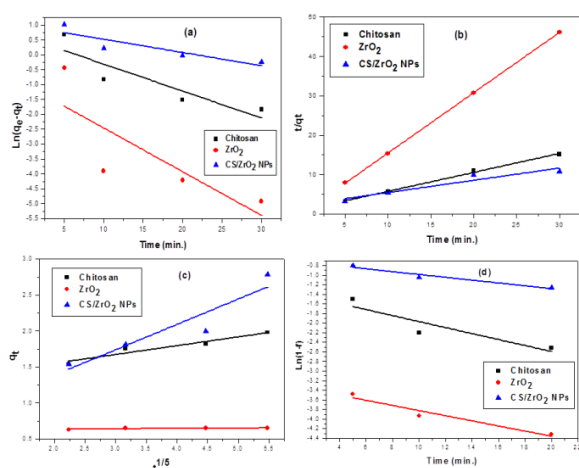


Figure (7) Kinetic models for chitosan, ZrO₂ and CS/ZrO₂ NCs at concentration 3 ppm a) Pseudo first order, b) Pseudo second order, c) Inter-particle diffusion and d) Liquid film diffusion models.

3.2.6 Adsorption mechanism

3.2.6.1. Intraparticle diffusion

Once adsorbed on the surface, solute particles diffuse into the pores on the surface of adsorbent and form bonding, which may be the rate determining step. For an adsorbing system the straight line should pass through the origin and the intercept value provides an idea about the deviation from intraparticle diffusion model or contribution of the film diffusion mechanism [44]. The value of Intraparticle diffusion rate coefficient (k_{ipd}) for chitosan, ZrO₂ and CS/ZrO₂ NCs adsorption were observed to be 0.35, 0.11 and 0.47 mg/g min^{0.5} at 3 ppm Fig. (7-c). Plots were straight line but did not pass through the origin and had intercepts of 0.36, 0.17 and 0.19 at 3 ppm, which suggested that adsorption of RB dye did not depend on intraparticle diffusion step. The intraparticle process depends on the size of the particle to be adsorbed and size of the pores on the surface of the three adsorbents.

3.2.6.2. Liquid film diffusion

The liquid film diffusion model was employed to investigate whether interface between solid and aqueous phase played a role during the transportation of the adsorbate from solution to the adsorbent. If film diffusion is rate controlling step, then the rate will depend on the thickness of film surrounding the adsorbent particle. The values of film diffusion rate coefficient $k_{fd} = 0.12$ g/g min for chitosan with intercept -0.54, $k_{fd} = 0.7$ g/g min for ZrO₂ with intercept 0.01 and $k_{fd} = 0.06$ g/g min for CS/ZrO₂ NCs with intercept -0.28. The insignificant non-zero intercept values indicated that the dye removal may be followed by film diffusion mechanism. Smaller deviations might be due to the shear on the particles during agitation, which considerably reduced the thickness of the aqueous layer surrounding the particles. Thus boundary layer resistance or film diffusion might be rate-limiting step in RB adsorption.

4. Conclusions

In the present work, Chitosan nano particles and Chitosan loaded ZrO₂ nano composite were prepared and applied for the removal of the Rose Bengal dye (RB) from aqueous solution. Adsorption isotherms well fitted in the adsorption data for RB dye to Freundlich model. The results obtained from kinetics revealed that, the pseudo-second order was the better model referring to the chemical adsorption mechanism for dye removal. Current results show that, 30%ZrO₂ loaded Chitosan is efficient for RB removal from waste water.

5. Conflicts of interest

There are no conflicts to declare.

Adsorbent	Conc. ppm	Pseudo first-order model			Pseudo second-order model				Intraparticle diffusion model			Liquid film diffusion		
		$q_{e,1,cal}$ (mg/g)	K_1 (min^{-1})	R^2	$q_{e,2,cal}$ (mg/g)	K_2 (g/mg min)	h (mg/g min)	R^2	K_{int} ($\text{mg/g min}^{0.5}$)	C (mg/g)	R^2	K_{fd}	C	R^2
Chitosan	50	20.25	0.063	0.98	178.6	0.004	0.71	0.93	3.44	-2.11	0.93	0.06	0.08	0.98
	30	19.05	0.095	0.98	57.14	0.015	0.85	0.59	3.22	-1.38	0.96	0.09	0.13	0.98
	15	9.02	0.106	0.99	13.00	0.065	0.85	1.00	1.62	-0.09	0.99	0.11	0.05	0.99
	7	4.44	0.124	0.97	5.65	0.094	0.53	0.98	0.78	0.09	0.99	0.12	0.07	0.97
	3	1.16	0.116	0.79	2.08	0.509	1.06	1.00	0.35	0.36	0.82	0.12	-0.54	0.79
ZrO ₂	50	5.94	0.19	0.88	8.10	0.19	1.54	0.97	1.30	0.58	0.88	0.19	-0.13	0.88
	30	5.00	0.12	0.82	7.58	0.21	1.57	0.99	1.21	0.62	0.91	0.12	-0.27	0.82
	15	2.08	0.17	0.84	3.56	0.59	2.11	1.00	0.61	0.60	0.82	0.17	-0.48	0.84
	7	0.36	0.19	0.58	1.56	5.26	8.18	1.00	0.27	0.41	0.68	0.19	-1.46	0.58
	3	0.65	0.70	1.00	0.65	16.58	10.8	1.00	0.11	0.17	0.68	0.70	0.01	1.00
CS/ZrO ₂	50	28.14	0.11	0.95	38.76	0.19	7.52	0.99	6.01	3.38	0.94	0.11	-0.17	0.95
	30	12.16	0.10	0.69	23.36	0.50	11.72	0.99	3.85	4.20	0.80	0.10	-0.61	0.69
	15	6.78	0.08	0.61	13.11	0.43	5.62	0.99	2.13	2.30	0.80	0.08	-0.62	0.61
	7	5.00	0.15	0.95	6.78	0.33	2.22	1.00	1.10	0.92	0.87	0.15	-0.21	0.95
	3	2.11	0.06	0.78	3.22	0.13	0.43	0.91	0.47	0.19	0.95	0.06	-0.28	0.78

(Table 4) Kinetic parameters RB on chitosan, ZrO₂ and CS/ZrO₂ NCs in aqueous solution

6. Acknowledgment

This paper is based upon work supported by Science, Technology & Innovation Funding Authority (STDF) under grant number (44848)

7. References

- Zhang, J., Ding, E., Xu, S., Li, Z., Fakhri, A., & Gupta, V. K., Production of metal oxides nanoparticles based on poly-alanine/chitosan/reduced graphene oxide for photocatalysis degradation, anti-pathogenic bacterial and antioxidant studies. *International Journal of Biological Macromolecules*, 164, 1584-1591 (2020). DOI: 10.1016/j.ijbiomac.2020.07.291
- Ait Ahsaine, H., Anfar, Z., Zbair, M., Ezahri, M., & El Alem, N., Adsorptive removal of methylene blue and crystal violet onto micro-mesoporous Zr₃O/activated carbon composite: A joint experimental and statistical modeling considerations. *Journal of chemistry*, vol.2018, article ID 6982014, 14 pages, 2018. DOI:10.1155/2018/6982014
- Soleiman Rahmani, Behzad Zeynizadeh, Shiva Karami, Removal of cationic methylene blue dye using magnetic and anionic cationic modified montmorillonite: kinetic, isotherm and thermodynamic studies, *Applied Clay Science*, 184, 105391, (2020). DOI:10.1016/j.clay.2019.105391
- Das, L., Das, P., Bhowal, A., & Bhattacharjee, C., Synthesis of hybrid hydrogel nano-polymer composite using Graphene oxide, Chitosan and PVA and its application in waste water treatment. *Environmental Technology & Innovation*, 18, 100664. (2020). DOI: 10.1016/j.eti.2020.100664
- Ahmed Ibrahim; Gomaa Farouk El Fawal; Magda A. Akl. "Methylene Blue and Crystal Violet Dyes Removal (As A Binary System) from Aqueous Solution Using Local Soil Clay: Kinetics Study and Equilibrium Isotherms". *Egyptian Journal of Chemistry*, 62, 3, 541-554, (2019). doi: 10.21608/ejchem.2018.4113.1360
- Faiq F. Karam; Noor H.M. Saeed; Ahmed Al Yasasri; Luma Ahmed; Hind Saleh. "Kinetic Study for Reduced the Toxicity of Textile Dyes (Reactive yellow 14 dye and Reactive green dye) Using UV-A light/ZnO System". *Egyptian Journal of Chemistry*, 63, 8, 2987-2998, (2020). doi: 10.21608/ejchem.2020.25893.2511
- Mohamed S. Yahia, Ahmed S. Elzaref. Magdy B. Awad, Ahmed M. Tony and Ahmed S. Elfeky, Efficient adsorption of chlorpyrifos onto modified activated carbon by gamma irradiation; a plausible adsorption mechanism, *Zeitschrift für Physikalische Chemie*, vol. 236, no. 1, 1-25, (2021). DOI: 10.1515/zpch-2020-1765.
- Baghapour MA, Djahed B, Ranjbar M. Removal of Methylene Blue from aqueous solutions. *J Health Sci Surveillance Sys*, vol. 1(1):48-56, (2013).
- Saheed, I.O., Adekola, F.A., Olatunji, G.A., Sorption study of methylene blue on activated carbon prepared from Jatropha curcas and Terminalia catappa seed coats. *J. Turk. Chem. Soc. A: Chem.* 4, 375–394, (2017). DOI: 10.18596/JOTCSA.287337
- Bao, Y., Zhang, G., Study of adsorption characteristics of methylene blue onto activated carbon made by Salix Psammophila. *Energy Procedia* 16, 1141–1146, (2012). DOI: 10.1016/j.egypro.2012.01.182
- Zhang, F., Song, W., Lan, J., Effective removal of methyl blue by fine-structured strontium and barium phosphate nanorods. *Appl. Surf. Sci.* 326, 195–203, (2015). DOI: 10.1016/j.apsusc.2014.11.143
- Upadhyayula, V.K., Deng, S., Mitchell, M.C., Smith, G.B., Application of carbon nanotube technology for removal of contaminants in drinking water: a review. *Sci. Total Environ.* 408, 1–13. (2009). DOI: 10.1016/j.scitotenv.2009.09.027
- Rocher, V., Siaugue, J.-M., Cabuil, V., Bee, A., Removal of organic dyes by magnetic alginate beads. *Water Res.* 42, 1290–1298, (2008). DOI: 10.1016/j.watres.2007.09.024
- Lackovičová, M., Baranyaiová, T., Bujdák, J., The chemical stabilization of methylene blue in colloidal dispersions of smectites. *Appl. Clay Sci.* 181 (article No. 105222), (2019). DOI: 10.1016/j.clay.2019.105222
- Wu, T., Cai, X., Tan, S., Li, H., Liu, J., Yang, W., Adsorption characteristics of acrylonitrile, p-toluenesulfonic acid, 1-naphthalenesulfonic acid and methyl blue on graphene in aqueous solutions. *Chem. Eng. J.* 173, 144–149, (2011). DOI.org/10.1016/j.cej.2011.07.050
- Ahmed Samer Elfeky, Hanan Farouk Youssef and Ahmed Shafek Elzaref, Adsorption of Dye from Wastewater onto ZnO Nanoparticles-Loaded Zeolite: Kinetic, Thermodynamic and Isotherm Studies, *Zeitschrift für Physikalische Chemie*, vol.234, no. 2, 255-278, (2020). DOI:10.1515/zpch-2018-1342
- Ghorai, S., Sarkar, A., Raoufi, M., Panda, A.B., Schönherr, H., Pal, S., Enhanced removal of methylene blue and methyl violet dyes from aqueous solution using a nanocomposite of hydrolyzed polyacrylamide grafted xanthan gum and incorporated nanosilica. *ACS Appl. Mater. Interfaces* 6, 4766–4777, (2014). <https://doi.org/10.1021/am4055657>

18. Kean, T & Thanou, M. Biodegradation, biodistribution and toxicity of chitosan. *Advanced drug delivery reviews*, 62(1), 3-11(2010). DOI: 10.1016/j.addr.2009.09.004
19. Fang Tian, Weiliang Chen, Cai'E Wu, Xiaohong Kou, Gongjian Fan, Tingting Li, Zhihao Wu, Preservation of ginkgo (*Ginkgo biloba* L.) seeds by coating with chitosan/nano-TiO₂ and chitosan/nano-SiO₂ films, *Biomac*, 12,177, (2018) DOI: 10.1016/j.ijbiomac.2018.12.177
20. Hosni Mahmoud, Sami & Salama, D.M. & Abd El-Aziz, M., Effect of chitosan and chitosan nanoparticles on growth, productivity and chemical quality of green snap bean. *Bioscience Research*. Vol. 15. 4307-4321, (2018).
21. El-Mohamedya, R. S. R., M. E. Abd El-Aziz, and S. Kamel, Antifungal activity of chitosan nanoparticles against some plant pathogenic fungi in vitro. *Agricultural Engineering International: CIGR Journal*, 21(4): 201–209, (2019).
22. El-Sayed, H.S., El-Sayed, S.M., Mabrouk, A.M.M. et al. Development of Eco-friendly Probiotic Edible Coatings Based on Chitosan, Alginate and Carboxymethyl Cellulose for Improving the Shelf Life of UF Soft Cheese. *J Polym Environ* 29, 1941–1953 (2021). <https://doi.org/10.1007/s10924-020-02003-3>
23. Abd El-Aziz, M.E., Youssef, A.M., Kamel, S. et al. Conducting hydrogel based on chitosan, polypyrrole and magnetite nanoparticles: a broadband dielectric spectroscopy study. *Polym. Bull.* 76, 3175–3194 (2019). <https://doi.org/10.1007/s00289-018-2545-1>
24. Dhakshinamoorthy, Amarajothi et al. "Pristine and modified chitosan as solid catalysts for catalysis and biodiesel production: A minireview." *International journal of biological macromolecules* vol. 167, 807-833, (2021). DOI:10.1016/j.ijbiomac.2020.10.216
25. H. El Knidri, R. Belaabed, A. Addaou, A. Laajeb, A. Lahsini, Extraction, chemical modification and characterization of chitin and chitosan, *Int. J. Biol. Macromol.* 120, 1181-1189, (2018). DOI: 10.1016/j.ijbiomac.2018.08.139
26. Qamar, S. A., Ashiq, M., Jahangeer, M., Riasat, A., & Bilal, M., Chitosan-based hybrid materials as adsorbents for textile dyes—A review. *Case Studies in Chemical and Environmental Engineering*, 100021, (2020). DOI: 10.1016/j.cscee.2020.100021
27. Dong-Wan Cho, Byong-Hun Jeon, Yoojin Jeong, In-Hyun Nam, Ui-Kyu Choi, Rahul Kumar, Hocheol Song, Synthesis of Hydrous Zirconium Oxide-Impregnated Chitosan Beads and Their Application for Removal of Fluoride and Lead., *Applied Surface Science*, vol. 372, 13-19, (2016). <https://doi.org/10.1016/j.apsusc.2016.03.068>
28. Jiang, H., Chen, P., Luo, S. et al. Synthesis of Novel Biocompatible Composite Fe₃O₄/ZrO₂/Chitosan and Its Application for Dye Removal. *J Inorg Organomet Polym* 23, 393–400, (2013). <https://doi.org/10.1007/s10904-012-9792-7>
29. Ch Venkata Reddy, I. Neelakanta Reddy, K. Ravindranadh, Kakarla Raghava Reddy, Nagaraj P. Shetti, D. Kim, J. Shim, Tejraj M. Aminabhavi, Copper-doped ZrO₂ nanoparticles as high-performance catalysts for efficient removal of toxic organic pollutants and stable solar water oxidation, *Journal of Environmental Management*, vol.260, 110088, (2020). <https://doi.org/10.1016/j.jenvman.2020.110088>
30. Mohammed Eid M. Ali; Shimaa M. Abdel Moniem; Hanan S. Ibrahim; Nabila S. Ammar; Heba K. El-Kholly; M.H. Helal; Ahmed G. El-Deen; M.K. Zahran. "Production of zirconia materials from zircon for dye removal from wastewater". *Egyptian Journal of Chemistry*, 63, 2, 515-523, (2020). doi: 10.21608/ejchem.2019.13583.1838
31. S. Salehi, S. Alijani and M. Anbia, Enhanced adsorption properties of zirconium modified chitosan-zeolite nanocomposites for vanadium ion removal, *International Journal of Biological Macromolecules*, vol. 164, 105-120, (2020). DOI: 10.1016/j.ijbiomac.2020.07.055
- Wu, Y., Zhang, Y., Lv, X., Mao, C., Zhou, Y., Wu, W & Huang, Z., Synthesis of polymeric ionic liquids microspheres/Pd nanoparticles/CeO₂ core-shell structure catalyst for catalytic oxidation of benzyl alcohol. *Journal of the Taiwan Institute of Chemical Engineers*, 107, 161-170, (2020). <https://doi.org/10.1016/j.jtice.2019.11.006>
32. Qi LF, Xu ZR, Li Y, Jiang X, Han XY. In vitro effects of chitosan nanoparticles on proliferation of human gastric carcinoma cell line MGC803 cells. *World J Gastroenterol*, 11(33), 5136-5141, (2005). DOI:10.3748/wjg.v11.i33.5136
33. R: A. M. Studer, L. K. Limbach, L. Van Duc et al., "Nanoparticle cytotoxicity depends on intracellular solubility: comparison of stabilized copper metal and degradable copper oxide nanoparticles," *Toxicology Letters*, vol. 197, no. 3, pp. 169–174, (2010). DOI:10.1016/j.toxlet.2010.05.012
34. Badriah Saad Al-Farhan, Characterization of ZrO₂ Nano Particles Prepared by Glycothermal Method and their Efficiency as Adsorbent of As(III) and As(V) from Waste Water, *Journal of Environmental & Analytical Toxicology*, 7,6, 1000532, (2017). DOI: 10.4172/2161-0525.1000532

35. NCHorti^{1,2}, MDKamatagi^{1,5}, SKNataraj³, MNWari⁴ and SR Inamdar⁴, Structural and optical properties of zirconium oxide (ZrO₂) nanoparticles: effect of calcination temperature, *Nano Express* 1, 010022, (2020). <https://doi.org/10.1088/2632-959X/ab8684>
36. Yanping Zhu, Naiyun Gao, Qiongfang Wang, Xingya Wei, Adsorption of perchlorate from aqueous solutions by anion exchange resins: Effects of resin properties and solution chemistry, *Colloids and Surfaces A: Physicochemical and Engineering Aspects*, vol. 468, 114–121, (2015). <https://doi.org/10.1016/j.colsurfa.2014.11.062>
37. Mary Jenish Barnabas, Surendran Parambadath, Aneesh Mathew, Sung Soo Park, Ajayan Vinu, Chang-Sik Ha, Highly efficient and selective adsorption of In³⁺ on pristine Zn/Al layered double hydroxide (Zn/Al-LDH) from aqueous solutions, *Journal of Solid State Chemistry*, vol. 233 133–142, (2016). <https://doi.org/10.1016/j.jssc.2015.10.001>
38. A. Swelam, M. Awad, A. Salem, A. El-Feky, An economically viable method for the removal of cobalt ions from aqueous solution using raw and modified rice straw, *HBRC. J.*, vol. 14, 255-262, (2018). <https://doi.org/10.1016/j.hbrej.2016.10.001>
39. D. Zhuhong, H. Xin, W. Yongshan, W. Shengsen, G. Bin, Removal of lead, copper, cadmium, zinc, and nickel from aqueous solutions by alkali-modified biochar: Batch and column tests, *Journal of Industrial and Engineering Chemistry*, vol. 33, 239–245, (2016). <https://doi.org/10.1016/j.jiec.2015.10.007>
40. S. Congcong, C. Chen, T. Wen, Z. Zhao, X. Wang, A. Xu, Superior adsorption capacity of g-C₃N₄ for heavy metal ions from aqueous solutions, *Journal of Colloid and Interface Science*, vol. 456, 7–14, (2015). <https://doi.org/10.1016/j.jcis.2015.06.004>
41. Moaaz K. Seliem, Sridhar Komarneni, Mostafa R. Abu Khadra, Phosphate removal from solution by composite of MCM-41 silica with rice husk: Kinetic and equilibrium studies, *Microporous and Mesoporous Materials*, vol. 224, 51–57, (2016). <https://doi.org/10.1016/j.micromeso.2015.11.011>
42. Saif A. Chaudhry, Tabrez A. Khan & Imran Ali, Adsorptive removal of Pb(II) and Zn(II) from water onto manganese oxide-coated sand: Isotherm, thermodynamic and kinetic studies, *Egyptian Journal of Basic and Applied Sciences*, 3:3, 287-300, (2016). DOI: 10.1016/j.ejbas.2016.06.002
43. A.S. Elfeky, H.F. Youssef, A.S. Elzaref, "Adsorption of Dye from Wastewater onto ZnO Nanoparticles-Loaded Zeolite: Kinetic, Thermodynamic and Isotherm Studies" *Zeitschrift für Physikalische Chemie*, vol. 234, no. 2, pp. 255-278, (2020). <https://doi.org/10.1515/zpch-2018-1342>